



# Environmental factors contributing to variations in CO<sub>2</sub> flux over a barley–rice double-cropping paddy field in the Korean Peninsula

Changhyoun Park<sup>1</sup> · Tarek S. El-Madany<sup>2</sup> · Soon-Hwan Lee<sup>3</sup>

Received: 21 February 2022 / Revised: 17 June 2022 / Accepted: 22 July 2022  
© The Author(s) under exclusive licence to International Society of Biometeorology 2022

## Abstract

Understanding the CO<sub>2</sub> flux over agricultural crop fields is critical because the temporal cycle is driven by both ecological environment and anthropogenic change. We analyzed the net ecosystem exchange of CO<sub>2</sub> measured over a barley–rice double-cropping field using the eddy covariance method for 5 years. We conducted gap-filling based on  $u_*$ -threshold criteria and partitioned the net ecosystem exchange into gross primary production and respiration. The relative importance analysis of solar radiation, temperature, soil heat flux, soil water content, and vapor deficit revealed that solar radiation and temperature were the dominant contributors to net ecosystem exchange. The annual variation in the net ecosystem exchange followed a bimodal pattern driven by CO<sub>2</sub> uptake by both barley and rice, displaying two negative peaks in late April and mid-August. The elongation stages of the crops exhibited the highest flux. Gross primary production and respiration were closely related to solar radiation and nighttime temperature, respectively. The relative importance of the other environmental variables was affected by the cultivation season and irrigation water. In the period of rice cultivation, respiration was approximately  $3 \mu\text{mol m}^{-2} \text{s}^{-1}$  higher during rice drainage than during the flooded period. The accumulated net ecosystem production was estimated to be  $315 \text{ gC m}^{-2}$  and  $349 \text{ gC m}^{-2}$  for the barley and rice growing periods, respectively, and  $649 \text{ gC m}^{-2}$  for the annual total. These values are comparable with the results of other studies on barley–rice double-cropping fields.

**Keywords** CO<sub>2</sub> fluxes · Gross primary production · Ecosystem respiration · Flux partitioning · Barley · Rice double-cropping field · Relative importance analysis

## Introduction

The main anthropogenic drivers of climate change are activities such as the burning of fossil fuels and land use, which lead to an increase in greenhouse gasses (GHGs) and aerosol concentrations (IPCC, 2021). The escalation of GHG levels can increase the absorption of longwave radiation from the earth's surface and raise air temperature, ultimately accelerating global warming. Carbon exchange is affected by the

use of fossil fuels and changes in land use and land cover, which are primarily caused by urbanization, deforestation, and cultivation (Pielke et al., 2011).

The terrestrial surface and the atmosphere continuously exchange energy, mass, and momentum, thereby affecting life on earth. The increase in carbon mass in the air can affect the earth's ecosystem; therefore, the quantification of the exchange of CO<sub>2</sub> is important. The interaction of CO<sub>2</sub> between the terrestrial surface and the atmosphere can be expressed by net ecosystem exchange (NEE), which is the vertical CO<sub>2</sub> flux from the ecosystem to the atmosphere, and can be partitioned into gross ecosystem exchange (GPP) minus respiration (Re). The NEE, GPP, and Re can be affected by both meteorological and environmental variables, including solar radiation, temperature, soil moisture, phenology, and nutrition (Bhatia et al., 2012; Saito et al., 2009; Schmitt et al., 2010; Powell et al., 2006).

Three methods of quantifying CO<sub>2</sub> flux have been established: (1) analysis of carbon content of crop and soil types

✉ Soon-Hwan Lee  
withshlee@pusan.ac.kr

<sup>1</sup> Institute of Environmental Studies, Pusan National University, Busan, South Korea

<sup>2</sup> Department of Biogeochemical Integration, Max Planck Institute for Biogeochemistry, Jena, Germany

<sup>3</sup> Department of Earth Science Education, Pusan National University, Busan, South Korea

(Arevalo et al., 2011; Smith et al., 2020), (2) measurement of the variation of carbon concentration in a constant volume chamber within a certain period (Chaichana et al., 2018; Meijide et al., 2020; Poyda et al., 2017; Schneider et al., 2012), and (3) measurement of the flux of carbon exchange using the eddy covariance (EC) system (Baldocchi, 2020; Prescher et al., 2010; Testi et al., 2008; Wohlfahrt and Galvagno, 2017). The EC system can be used to conduct long-term continuous vertical flux measurements over relatively large areas without significantly damaging or changing the environment. Globally, more than 500 flux measurement sites are in operation over forests, grasslands, wetlands, and croplands on a long-term basis under the FLUXNET network (Baldocchi et al., 2001; Falge et al., 2002) as well as in urban areas (Park and Schade, 2016; Velasco et al., 2013). Among the wide variety of global terrestrial ecosystems, most flux measurements have focused on forests due to their extensive coverage (~28% of the global land area), compared to other land cover types, such as crops (~12%) or the combination of grasslands and open-woodlands (~35%) (Kanianska, 2016).

Agricultural lands play a significant role in the production of heterotrophic energy, human food security, and regional and global CO<sub>2</sub> budgets. Crops mainly uptake CO<sub>2</sub> from the atmosphere and store it via photosynthesis, releasing it back into the atmosphere via respiration (Re). Rice paddy fields also release methane (CH<sub>4</sub>) into the atmosphere through the anaerobic decomposition of soil organic matter. Based on the statistics of the Food and Agriculture Organization of the United Nations (FAO; <http://www.fao.org/faostat>), maize is the most produced crop worldwide, followed by rice, wheat, and barley. Rice is the primary cereal produced in Asia, and the rice cultivation area accounts for over 90% of the global rice cultivation areas (<https://www.fao.org/3/x6905e/x6905e04.htm>). Rice cultivation is very labor-intensive and requires substantial amounts of water and heat, as well as humid weather conditions; therefore, flooded fields (called paddies) are commonly used. Barley is mainly consumed in Asia and spans over a vast geographic area of cultivation. From 2006 to 2008, barley was cultivated from mountaintops to seacoasts and from the tropics to high latitudes, covering approximately 56 million ha across 106 countries (Newton et al., 2011).

The EC method has been used to measure CO<sub>2</sub> flux over crop fields, and seasonal and annual variations in flux over rice paddy fields have been reported in Japan (Miyata et al., 2000, 2005; Saito et al., 2005), the Philippines (Alberto et al., 2009), Taiwan (Tseng et al., 2010), China (Ren et al., 2007), and Korea (Hong et al., 2001; Moon et al., 2003). Conversely, there are few studies on barley fields in Germany (Moyano et al., 2007) and Finland (Lohila et al., 2004). Because of the increase in air temperature in winter, which can significantly affect the carbon flux, barley–rice

double-cropping regions have expanded worldwide, based on the OECD statistics data ([https://stats.oecd.org/Index.aspx?DataSetCode=LAND\\_USE](https://stats.oecd.org/Index.aspx?DataSetCode=LAND_USE)). Studies have been conducted on rotational crop fields in Japan (Takimoto et al., 2010) and Korea (Kwon et al., 2010; Min et al., 2014; Shim et al., 2014, 2016). To the best of our knowledge, these are the only studies focusing on barley–rice double-cropping fields.

This study aimed to (1) introduce our ground-level CO<sub>2</sub> flux measurement system at the Boseong Standard Weather Observatory (BSWO), which is not currently affiliated with FLUXNET; (2) describe the relationship of CO<sub>2</sub> flux, including the NEE, GPP, and Re related environmental factors; and (3) report on the long-term CO<sub>2</sub> flux over barley–rice double-cropping fields, which is rare in current flux research.

## Methods

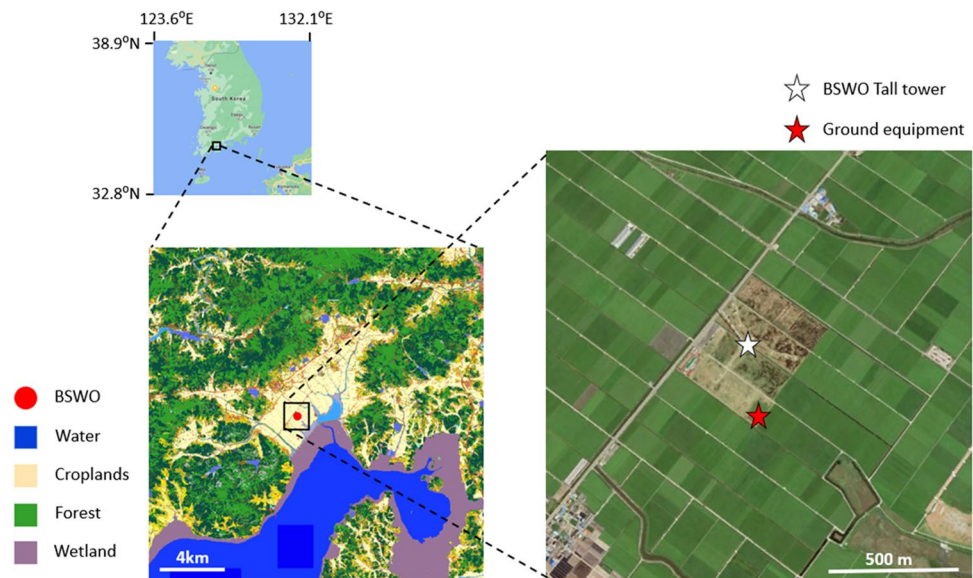
### Site description

The flux measurement site is located in the middle of a flat homogeneous barley–rice double-cropping paddy fields (3 m above sea level) in Boseong-gun County, Jeollanam-do Province, South Korea. The measurement point was established at the edge of the observation field of the BSWO (34°45'48" N, 127°12'53" E) run by the National Institute of Meteorological Sciences of Korea. A brief introduction to the BSWO is provided in the Supplemental information (SI). Around the study site, the Namhae coast is located approximately 1.5 km southeast of the site and mountains (576 m in height) are located to the north and stretch to the northeast (Fig. 1). Agricultural warehouses and residential houses are located to the west and northeast near the mountain foot. Two single-lane roads cross the mountain foot from the northeast to the southwest, approximately 1.5 km north of the site. Barley and rice crop fields cover approximately 3500 ha of the basin.

### Cultivation phases

The main crops planted around the study site are barley (*Hordeum vulgare*) and rice (*Oryza sativa*), which are planted yearly via the double-cropping cultivation method. The barley cultivation period (BAR) began with sowing in early November. Seed germination begins with the emergence of seedling roots, and seedlings undergo winter dormancy until early February. The stem then elongates, followed by booting, head emergence, flowering, and milk and dough development in the kernel from mid-February to early May. The growth continues with ear formation, flowering, and grain filling until mid-May and ends with ripening in late May. We classified the growth of crops into four stages,

**Fig. 1** Location of the study area and the distribution of land cover retrieved from the geographic information system (GIS). The locality and ground measurement equipment are shown in Supplementary Fig. 1



focusing on the seasonal variations in  $\text{CO}_2$  flux: germination (or emergence;  $B_1$ ); tillering ( $B_2$ ) including seedling and winter rest; elongation ( $B_3$ ) including stem elongation, ear formation, flowering, ripening ( $B_4$ ), and harvesting ( $B_h$ ).

The rice cultivation period (RIC) can also be divided into four stages depending on the status of growth: transplanting and rooting ( $R_1$ ), seedling development (or tillering,  $R_2$ ), growth (elongation,  $R_3$ ), ripening ( $R_4$ ), and harvesting stages ( $R_h$ ). The RIC begins with transplanting rice seedlings into the paddy field in early June. The seedlings experience tillering and leaf formation until mid-July. In  $R_3$ , the rice stems elongate, followed by booting and heading from mid-July to late August. Rice matures after anthesis in late August. Harvesting begins in late October. Rice requires copious water to grow; thus, farmers tend to flood their paddy fields constantly under 3–10 cm of water, during the so-called flooded period (FL). In this study period, the intermittent drained period (DR) occurred from July 31 to August 22, about 25–35 days before anthesis. We did not find a distinct fallow stage.

### Measurement equipment

The BSWO has a multilevel tall tower equipment for  $\text{CO}_2$  flux. As a follow-up study of our previous work on upper-levels (Park et al., 2021), we used ground-level data in this study. The measurement equipment was installed on a pole [2.6 m above ground level (a.g.l)] at the south edge of the observation field of the BSWO.

Temperature and humidity sensors (HMP155A, Vaisala), encapsulated by a radiation shield and a net radiation sensor (CNR<sub>4</sub>, Kipp & Zonen), were set up on the pole. A 3D sonic anemometer (CSAT3A, Campbell Sci.) was installed toward the east, combined with an open-path IRGA (EC150,

Campbell Sci.) for  $\text{CO}_2/\text{H}_2\text{O}$  measurements. The zero and span tests were performed for the calibration of IRGA at a week interval during the whole study period. Instruments for hydrometeorological measurements were set up on the east and west outer sides at the edge of the paddy field. A cosmic-ray soil moisture sensor (CRS1000, Hydroinnova, USA) was installed at 1.5 m a.g.l., and it was used to evaluate the spatial scaling of soil moisture by simultaneously performing area observations with wide spatial representation. Its calibration was executed based on soil samples, acquired at 6 points in grassland and 4 points in crop fields. Two soil moisture probes (CS616-L and CS-655L, Campbell Sci.) were set up 20 cm below the surface and measured soil water contents (SWCs). Soil heat flux (SHF) and temperature were measured 20 cm below the surface using an SHF plate (HFP01-L, Hukseflux) and a thermocouple probe (TCAV-L, Campbell Sci.), respectively.

### Data processing

The presented data spans over a period of 5 years (2016 to 2020). The sonic anemometer and IRGA raw data were recorded at 20 Hz using a data logger (CR3000, Campbell Sci.). EddyPro software (Licor; version 7.0.4) was used for the flux calculation, and the following settings and corrections were applied: The double rotation method (Wilczak et al., 2001) was followed to correct the anemometer axis tilt to mean streamlines, nullifying the averaged cross-stream and vertical components within a half-hour period. The block-averaging (or Reynolds averaging) method was used to calculate the turbulent fluctuations based on the method developed by Gash and Culf (1996). The WPL terms (Webb et al., 1980) were applied to compensate for density fluctuations in the open-path IRGA. Further raw data were analyzed

for despiking, drop-outs, skewness, and kurtosis based on Vickers and Mahrt (1997). The stationarity (steady state) test and the well-developed turbulence test were performed using the 0–1–2 quality flagging system, as suggested by Mauder and Foken (2006). We applied high- and low-frequency spectral corrections (Moncrieff et al., 1997, 2004). After producing 30-min average data, we removed the data during rain periods and 24 h after rain. Generally, 12 h is enough to remove water from open-path sensors. However, we need to make the analysis consistent with other flux measurement data, specifically acquired from closed-path sensors, which need more time to be dried up. These sensors were installed at higher levels of a tall tower in BSWO (Park et al., 2021). Wind direction data ranging from 30 to 240° was used, and the sectors affected by the tower structure and the grassland in the BSWO observation field were excluded.

To execute gap-filling and flux-partitioning with the 30-min averaged flux data, we used the “REddyProc” package (Wutzler et al., 2018) of the R statistical language software. The package performs a quality check and filtering based on several filters of estimated friction velocity ( $u_*$ ) thresholds to remove low turbulence data (Papale et al., 2006). During the study period, the seasonally averaged  $u_*$  thresholds ranged from 0.1 to 0.15 m s<sup>-1</sup>. The 30-min averaged data gap was filled based on shortwave radiation (R<sub>g</sub>), air temperature (T<sub>air</sub>), soil temperature (T<sub>soil</sub>), relative humidity (RH), and vapor pressure deficit (VPD). We used the nighttime-based method (Reichstein et al., 2005) to partition the NEE into GPP and Re. The data collection ratios for QA/QC and partitioning processes are listed in Supplementary Table 2. The measurement breaks before gap-filling occurred mainly because of system failures and maintenance requirements. The source areas of CO<sub>2</sub> flux can be determined using the footprint probability function, in which the spatial extent and intensity distribution are expression variables (Horst and Weil, 1992). We used a 2D online footprint parameterization model (Kljun et al., 2015) to calculate the footprints for each season.

We used the R-package “relaimpo” (Gromping, 2006) to perform a relative importance analysis (RIA) for identifying the drivers of flux among environmental variables, including R<sub>g</sub>, T<sub>air</sub>, T<sub>soil</sub>, SHF, and SWC, based on the method of El-Madany et al. (2020).

## Results and discussion

### Local climatology

The monthly average meteorological variables, including T<sub>air</sub>, T<sub>soil</sub>, RH, wind speed, R<sub>g</sub>, SHF, SWC, VPD, and accumulated rainfall, exhibited typical seasonal variations (Supplementary Fig. 2). The mean values of T<sub>air</sub> and T<sub>soil</sub>

were 25.1 °C and 26.5 °C in summer and 3.2 °C and 6.2 °C in winter, respectively. The average RH showed 80.2% in summer and 39.1% in winter, indicating hot, humid summers and cold, dry winters. Seasonal average wind speeds ranged from 2.0 to 2.9 m s<sup>-1</sup> during the whole study period. The dominant wind directions were south, southwest, and northwest, due to the complicated topography combined with the sea-land breeze around the site (Supplementary Fig. 3). The 5-year averaged total accumulated R<sub>g</sub> showed the highest and lowest values in August (465.90 MJ) and January (244.0 MJ), respectively. On average, SHF showed a positive value (5.84 W m<sup>-2</sup>) in summer and a negative value (−5.48 W m<sup>-2</sup>) in winter, indicating the direction of heat flux between the air and the ground depending on seasonal variations. The highest and lowest mean value of SWC appeared in September (0.31 m<sup>3</sup> m<sup>-3</sup>) and in December (0.23 m<sup>3</sup> m<sup>-3</sup>), with close relationships with seasonal rainfall and irrigation. Monthly averaged VPD ranged from 0.02 (June) to 0.10 (March), yet it showed no seasonal dependency. The monthly mean accumulated rainfall was significantly higher in summer (1222 mm) and lower in winter (240 mm), which is typical of the Korean Peninsula, owing to the effects of the Asian monsoon (from late June to mid-July) and typhoon (from late August to late September). Overall, the meteorological environment at the study site was suitable for barley–rice double-cropping.

### Flux source and uncertainty

We estimated the flux source areas with the online data processing tool for 2D flux footprint prediction (Kljun et al., 2015). The seasonal average 90% footprint probability is shown in Supplementary Fig. 4. The seasonally averaged footprint areas did not vary significantly from spring to autumn during the main barley and rice growing seasons. Most of the 90% footprint areas were within a ~0.2 km radius, covering the homogeneous crop field.

To estimate the flux uncertainty, we assessed the energy balance ratio [EBR = (R<sub>n</sub> − G)/(LE + H), where R<sub>n</sub>, H, LE, and G are the daily average radiation and sensible, latent, and SHF, respectively] (Wilson and Baldocchi, 2000). We calculated the daily average EBR and analyzed the regression between R<sub>n</sub> − G and LE + H using the daily average values in BAR and RIC (Supplementary Fig. 5). The EBR in BAR and RIC was 0.87 (RMSE: 34.08) and 0.82 (RMSE: 39.99), respectively, implying that LE + H was underestimated by ~13% and ~18% compared to R<sub>n</sub> − G in BAR and RIC, respectively. These values were within the range of EBR uncertainty suggested in a previous study (10–30% underestimation using the EC method) (Baldocchi, 2003; Stoy et al., 2013). Therefore, the quality of the measured CO<sub>2</sub> flux was acceptable for further analysis.

### Relative importance analysis

We also performed the analysis of variance (ANOVA) test for the GPP and Re with the linear equation:

$$y = \beta_0 + \beta_1 R_g + \beta_2 T_{air} + \beta_3 T_{soil} + \beta_4 SHF + \beta_5 + SWC + \beta_6 VPD + \varepsilon,$$

where  $y$  is GPP or Re in this test. The ANOVA table is in Supplementary Table 1. The results showed that the meteorological variables, including  $R_g$ ,  $T_{air}$ ,  $T_{soil}$ , SHF, SWC, and VPD, had significant effects on GPP and Re ( $p < 0.05$ ). The ANOVA table is reported in Supplementary Table 1.

We examined the relative importance of environmental variables affecting  $CO_2$  flux, including  $R_g$ ,  $T_{air}$ ,  $T_{soil}$ , SHF, SWC, and VPD. Figure 2 shows the contribution of the variables to the NEE for all day, GPP in daytime, and Re in nighttime, in the study period. Annually, the most significant driver for NEE was  $R_g$  ( $R^2 = 0.69$ ), followed by SHF ( $R^2 = 0.16$ ), temperature ( $R^2 = 0.07$ ,  $T_{air}$ ;  $R^2 = 0.06$   $T_{soil}$ ), SWC ( $R^2 = 0.01$ ), and VPD ( $R^2 = 0.01$ ). We observed that the SHF does not directly influence  $CO_2$  uptake and release but is regulated by the temporal variation of  $R_g$  (Supplementary Fig. 6). For GPP, the  $R^2$  for  $R_g$  and SHF was approximately 40% and 48% lower in RIC than in BAR and was associated with a 26% lower accumulated  $R_g$ . The contribution of  $R_g$

was about a factor of two lower in RIC than in BAR than that of temperature, and SHF mainly increased due to irrigated water. The relative importance of other environmental variables to GPP is discussed in later section.

For Re, the nighttime  $T_{air}$  was the essential variable in all cultivation periods, except for DR. During the day, the soil absorbed heat from  $R_g$  which was released into the atmosphere at night. The magnitude of the released heat was higher under drained conditions, resulting in a higher  $R^2$  of SHF than temperature. In FL, the contribution of temperature increased when the irrigated water lowered the SHF by converting  $R_g$  to latent heat.

### Temporal variation in flux

In this section, we discuss the temporal variation in flux, including the measured NEE, partitioned GPP, and Re. Supplementary Fig. 7 shows the daily average annual  $CO_2$  fluxes in each year. The largest negative peaks of NEE were observed around spring and summer, coinciding with the actively growing periods of barley and rice, respectively. The annual average NEE showed an increasing pattern from a minimum of  $-2.17 \mu mol m^{-2} s^{-1}$  in 2016 to a maximum of  $-1.18 \mu mol m^{-2} s^{-1}$  in 2020. The year 2017 was excluded from the analysis due to the lack of long-term data. The amplitude of flux was generally higher in BAR than in RIC

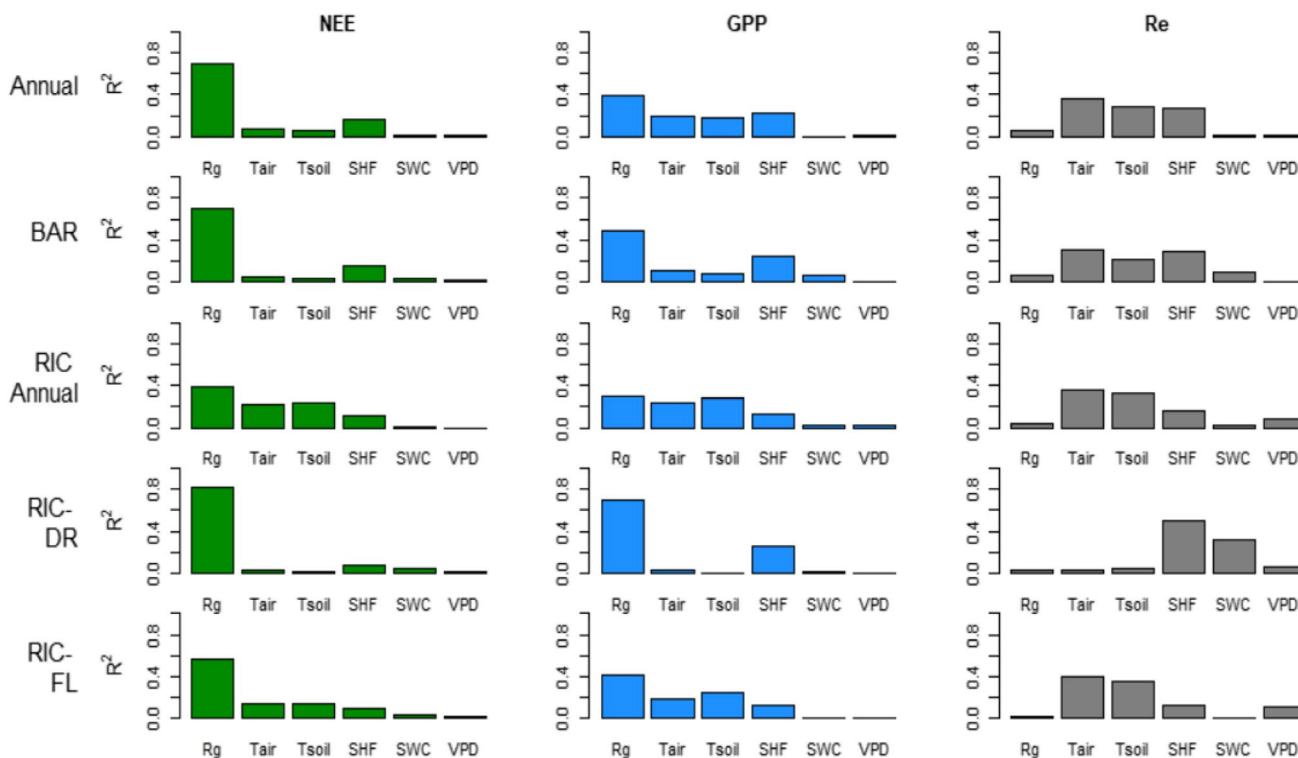


**Fig. 2** Relative importance of individual variables, including shortwave radiation ( $R_g$ ), air temperature ( $T_{air}$ ), soil temperature ( $T_{soil}$ ), soil heat flux (SHF), soil water content (SWC), and vapor pressure deficit (VPD), to NEE for all day, GPP during day, and Re during night

because of the higher  $T_{air}$  and  $R_g$  in RIC, except in 2020, due to the higher rainfall in summer (Supplementary Fig. 2).

The averaged flux on the same day of the year (DOY) was used to analyze the annual DOY variation. Hereafter, the averaged values in this method are called “DOY-mean.” Fig. 3 shows the annual variation in the daily average  $CO_2$  flux in relation to  $R_g$ ,  $T_{air}$ , SHF, and VPD. The mean values for each cultivation stage are presented in Table 1. The DOY-mean NEE, GPP, and  $Re$  showed bimodal patterns: The minimum NEE for BAR and RIC appeared on April 16 ( $-6.45 \mu mol m^{-2} s^{-1}$ ) and August 18 ( $-8.00 \mu mol m^{-2} s^{-1}$ ), respectively, showing strong  $CO_2$  uptake by crops.

For BAR, the DOY-mean NEE was positive ( $1.08 \mu mol m^{-2} s^{-1}$ ) in the germination stage ( $B_1$ ). In the seedling and winter-dormancy stage ( $B_2$ ), the NEE was  $0.09 \mu mol m^{-2} s^{-1}$  throughout the winter dormancy. Toward spring, the NEE gradually decreased from late  $B_2$  until the late elongation stage ( $B_3$ ) and rapidly increased throughout the ripening stage ( $B_4$ ) until harvesting. The DOY-mean uptake was the highest averaged value in  $B_3$  and decreased in  $B_4$  as the barley was ripening. Overall, the crop field acted as a net absorber during the BAR.

During RIC, the NEE showed a positive value ( $0.55 \mu mol m^{-2} s^{-1}$ ) in the rooting stage of rice ( $R_1$ ), mainly due to transplanting and heterotrophic soil  $Re$  due to low levels of photosynthesis by seedlings. The NEE became negative ( $-1.70 \mu mol m^{-2} s^{-1}$ ) during the tillering stage ( $R_2$ ), as the rice started to grow, and continued to decrease throughout the elongation stage ( $R_3$ ), which is the most active growing stage with a high net  $CO_2$  uptake. As anthesis began (the beginning of  $R_4$ ), the NEE increased until the completion of harvesting. There was a hump around late August, mainly due to the relatively lower  $R_g$  in relation to summer rainfall, which lowered  $CO_2$  absorption via photosynthetic activities. The effect of water in paddy fields will be discussed in later sections. Overall, the rice field acted as a net  $CO_2$  sink in BAR.

GPP is the difference between NEE and  $Re$ . The annual variation in the daily average GPP is likely a mirror image of the NEE at the stand of  $Re$  (Fig. 3); it displayed two peaks on April 16 ( $11.49 \mu mol m^{-2} s^{-1}$ ) and August 13 ( $16.66 \mu mol m^{-2} s^{-1}$ ). The GPP peaks in BAR and RIC appeared approximately 1 month later and earlier than that of the NEE, respectively, which was associated with the variability in  $Re$ . Except for the harvesting stages, the daily average GPP during the BAR was the highest in  $B_4$ , followed by  $B_3$ ,  $B_1$ , and  $B_2$ . During the RIC, the highest GPP appeared in  $R_3$ , followed by  $R_4$ ,  $R_2$ , and  $R_1$ . Overall, the average GPP in BAR and RIC was  $4.54 \mu mol m^{-2} s^{-1}$  and  $7.68 \mu mol m^{-2} s^{-1}$ , respectively, meaning that GPP in RIC was  $\sim 80\%$  higher than that in BAR. It seems  $R_g$  did not mainly cause this significant distinction because the average  $R_g$  did not show a large difference ( $< 15\%$ ) between BAR

and RIC (Fig. 3). The distinctive phenology of each crop can affect this difference, basically driven by fertilizer and water conditions. The leaf area index (LAI) can represent the phenology and be essential to estimating photosynthetic productivity by crop growth. Unfortunately, we did not have a chance to measure it during the study period.

The DOY-mean  $Re$  is mainly driven by seasonal variations in temperature. During the BAR, the variability in  $Re$  remained very low throughout  $B_1$  and  $B_2$  and then continuously increased until spring of the following year, reaching a maximum on May 2 ( $6.27 \mu mol m^{-2} s^{-1}$ ), when the barley was ripened and harvested. After rooting in  $R_1$ ,  $Re$  rapidly increased to a peak on August 5 ( $9.00 \mu mol m^{-2} s^{-1}$ ) in  $R_2$  and then began to gradually decrease until early winter. The highest daily average  $Re$  during the BAR occurred in  $B_4$ , followed by  $B_3$ ,  $B_1$ , and  $B_2$ ; however, the highest daily average  $Re$  during the RIC appeared in  $R_3$ , followed by  $R_4$ ,  $R_2$ , and  $R_1$ . Overall, the average  $CO_2$  released into the atmosphere during the BAR and RIC were  $3.13 \mu mol m^{-2} s^{-1}$  and  $5.51 \mu mol m^{-2} s^{-1}$ , respectively.

## Gross primary production

From the RIA, solar radiation is the dominant driver of GPP. The photosynthetically active radiation (PAR) sensors were not available at this site; thus, the measured shortwave incoming radiation was used to derive PAR. PAR is very closely correlated with shortwave radiation (Diak et al., 2004);  $PAR \sim SW/0.505$ , where the units of shortwave radiation and PAR are  $W m^{-2}$  and  $\mu mol m^{-2} s^{-1}$ , respectively.

The relationship between GPP and environmental variables, including PAR,  $T_{air}$ , SHF, SWC, and VPD, is shown in Fig. 4. GPP increased as PAR increased to approximately  $1800 \mu mol m^{-2} s^{-1}$  (the light saturation point) for both the BAR and RIC. We calculated the efficiency of  $CO_2$  uptake of each crop within the PAR range up to the light saturation point; rice absorbed approximately 20% more  $CO_2$  than barley. The linear regression slopes between GPP and PAR in each crop growth stage (Supplementary Fig. 8) showed that the highest  $CO_2$  absorption occurred in  $B_4$ , followed by  $B_3$ ,  $B_2$ , and  $B_1$  for BAR, and  $R_3$ , followed by  $R_4$ ,  $R_2$ , and  $R_1$  for RIC.

Although  $R_g$  is the single dominant driver for GPP, it is meaningful to investigate the relationship with other variables because their relative importance depends on the season, cultivation stage, and irrigation.  $T_{air}$  is distinct in BAR than in RIC, yet the increasing rate of GPP with SHF was similar in BAR and RIC-FL because irrigation significantly reduced SHF and decreased in early August (Fig. 3). The doubling of GPP in DR coincides with the peak of  $R_g$  in early August. Contrarily, the relationship with SWC (Fig. 4d) and VPD (Fig. 4e) showed a relatively flat pattern, and the amplitude range of GPP was limited to

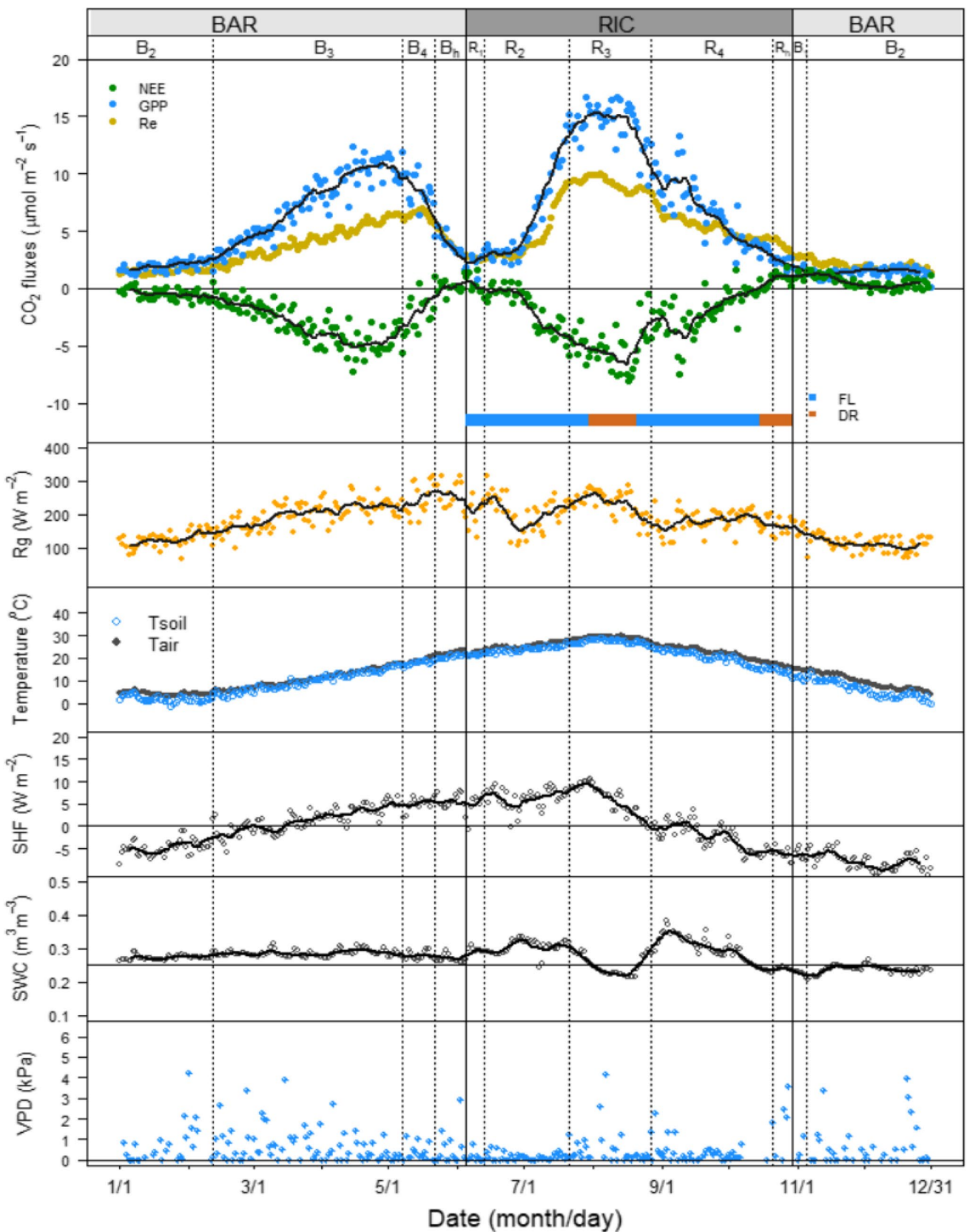


Fig. 3 DOY-mean CO<sub>2</sub> flux, in relation to Rg, temperature, SHF, SWC, and VPD. Black lines indicate the moving average

**Table 1** Average NEE, GPP, and Re in each crop cultivation stage

Crop type	Cultivation stage	Stage symbol	Fluxes ( $\mu\text{mol m}^{-2} \text{s}^{-1}$ )		
			NEE	GPP	Re
Barley	Germination	B <sub>1</sub>	1.08 ± 3.57	1.82 ± 4.04	2.9 ± 1.2
	Seedling and winter rest	B <sub>2</sub>	0.09 ± 3.6	1.68 ± 3.74	1.78 ± 0.87
	Elongation	B <sub>3</sub>	-3.14 ± 10.45	7.26 ± 11.26	4.12 ± 1.92
	Ripening	B <sub>4</sub>	-2.42 ± 11.16	8.83 ± 11.82	6.41 ± 1.6
	Harvesting	B <sub>h</sub>	0.22 ± 5.75	3.79 ± 6.1	4.00 ± 1.57
	Avg		-1.41 ± 9.18	4.54 ± 10.13	3.13 ± 2.46
Rice	Rooting	R <sub>1</sub>	0.55 ± 4.47	2.21 ± 4.51	2.76 ± 0.65
	Tillering	R <sub>2</sub>	-1.70 ± 8.65	5.96 ± 9.32	4.26 ± 1.97
	Elongation	R <sub>3</sub>	-5.27 ± 15.58	13.07 ± 16.23	7.75 ± 1.96
	Ripening	R <sub>4</sub>	-1.76 ± 9.68	6.42 ± 10.15	5.27 ± 1.85
	Harvesting	R <sub>h</sub>	1.08 ± 4.28	2.44 ± 4.64	3.91 ± 1.71
	Avg		-2.48 ± 11.12	7.68 ± 12	5.51 ± 2.39
Total	Avg		-1.66 ± 9.11	5.55 ± 10.05	4.08 ± 2.44

0–10  $\mu\text{mol m}^{-2} \text{s}^{-1}$  in BAR and FL, which explains the significantly lower contribution to GPP (Fig. 2). Under dry soil conditions, where the range of SWC was limited to 1.5–3  $\text{m}^3 \text{m}^{-3}$ , GPP was approximately double in DR than in FL.

## Respiration

Regulated by nighttime temperature,  $\text{CO}_2$  is usually released into the atmosphere via autotrophic and heterotrophic Re. The relationship between Re and temperature is typically assumed to be exponential, with a constant  $Q_{10}$  (temperature coefficient). Specifically, Re increases by a factor of 1.6–3 (mean value of ~2) with a 10 °C increase in temperature (Ryan, 1991).

Figure 5 displays the relationship between the daily average Re and nighttime  $T_{\text{air}}$  and  $T_{\text{soil}}$  at 2 °C intervals, and Supplementary Fig. 9 shows the scatter plots in each growing stage. Overall, Re exponentially increased with temperature during both BAR and RIC, as expected. The regression line can explain the relationship by more than 85%; thus, the NEE at night was dominated by Re. The  $Q_{10}$  for  $T_{\text{air}}$  and  $T_{\text{soil}}$  was 2.27 and 1.70 for BAR, 1.97 and 1.96 for RIC, and 1.93 and 1.73 annually, respectively. These values were comparable with the  $Q_{10}$  of 2.77 and 1.25 for BAR and RIC, respectively, as estimated by Takimoto et al. (2010) for a barley–rice double-cropping field in Japan.

The water keeps  $\text{CO}_2$  from being directly released into the atmosphere during FL, and the trapped  $\text{CO}_2$  can be emitted from the soil when the drainage starts (Nishimura et al., 2015; Saito et al., 2005; Shim et al., 2014). Lack of oxygen also plays an important role. If no oxygen enters the soil because of flooding, microbes reduce the carbon to methane. This may explain the reduction in  $\text{CO}_2$  production. Therefore,  $\text{CO}_2$  flux is expected to be lower during FL than during DR, especially at night. The Re exponentially increased

with temperature in FL, as expected, but the slopes changed in DR. With  $T_{\text{soil}}$  ranging from 20 to 30 °C, the average Re in DR (8.52  $\mu\text{mol m}^{-2} \text{s}^{-1}$ ) was higher than that in FL (5.26  $\mu\text{mol m}^{-2} \text{s}^{-1}$ ), which can indicate the active release of  $\text{CO}_2$  during DR, as described above. The difference between Re in DR and FL was ~3.26  $\mu\text{mol m}^{-2} \text{s}^{-1}$ , which can be interpreted as the mean potential  $\text{CO}_2$  flux trapped in the soil during FL. However, the EC method is limited in separating the sources of Re, such as anaerobic and aerobic Re, because the inlet of the EC system captures  $\text{CO}_2$  from both soil and crop leaves.

The Re values are comparable with soil Re measured in other barley–rice double-cropping fields: Shim et al. (2014) reported an average Re of 4.8  $\mu\text{mol m}^{-2} \text{s}^{-1}$  and 3.9  $\mu\text{mol m}^{-2} \text{s}^{-1}$  in DR and FL, respectively, in Gimje, South Korea; and Takimoto et al. (2010) suggested ~7  $\mu\text{mol m}^{-2} \text{s}^{-1}$  in Okayama, Japan. Based on soil chamber experiments performed over a rice field in Hubei, China, Liu et al. (2013) reported that Re ranged from -0.45 to 8.62  $\mu\text{mol m}^{-2} \text{s}^{-1}$ .

The RIA indicated that SHF was also relatively highly correlated with Re. Figure 6 shows the relationship between Re and SHF at night. The average Re increased with SHF (Fig. 6a) and was approximately 1.45  $\mu\text{mol m}^{-2} \text{s}^{-1}$  higher in RIC than in BAR. The temperature effect was controlled by maintaining the  $T_{\text{air}}$  from 20 to 30 °C, and the results are shown in Fig. 6b, which indicates a flat pattern in each cultivation period. This confirms that temperature rather than SHF was a direct controller of Re, as expected. The highest Re appeared in DR, followed by BAR and FL, and was mainly driven by the temporal variation of  $R_g$ . The difference was noticeable: The average Re was 8.76  $\mu\text{mol m}^{-2} \text{s}^{-1}$  and 5.08  $\mu\text{mol m}^{-2} \text{s}^{-1}$  in DR and FL, respectively, resulting from the active release of  $\text{CO}_2$  trapped during irrigation.

**Fig. 4** Relationship between GPP and environmental variables, including PAR, Tair, SHF, SWC, and VPD, using data binned into 100  $\mu\text{mol m}^{-2} \text{s}^{-1}$ , 2  $^{\circ}\text{C}$ , 4  $\text{W m}^{-2}$ , 0.5  $\text{m}^3 \text{m}^{-3}$ , and 0.5 kPa intervals, respectively. Error bars indicate the 1-sigma standard deviation of all flux data in each bin

### Annual CO<sub>2</sub> budget

To estimate the annual budget of CO<sub>2</sub> and suggest the quantified data for flux-related communities, we calculated the annual total net ecosystem production (NEP = -NEE), GPP, and Re, as displayed in Fig. 7. The annual NEP decreased by approximately 5% every year except for 2017. Until 2019, the annual GPP likely retained a value of about 2200  $\text{gC m}^{-2}$ , while the annual Re gradually increased. The former and the latter ~ 13% and ~ 15%, respectively, decreased in 2020, in which Rg was lower because of the higher accumulated rainfall in summer. The NEP ranged from 557  $\text{gC m}^{-2}$  (2020) to 786  $\text{gC m}^{-2}$  (2016) during the study period, excluding 2017.

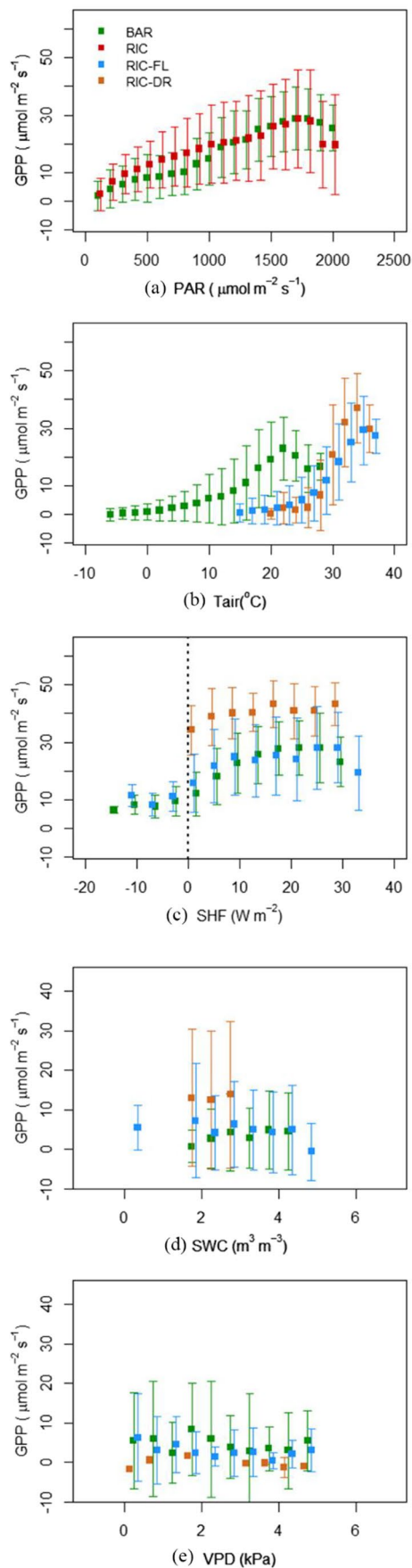
The annual flux was compared with the results of other studies, as shown in Table 2. To our knowledge, only five studies have been conducted using EC methods in barley–rice double-cropping fields. The average NEP in the BAR (315  $\text{gC m}^{-2}$ ) was ~ 10% lower than that reported by Min et al. (2014). In RIC, the average NEP (349  $\text{gC m}^{-2}$ ) was within the range reported by Shim et al. (2014, 2016). The NEP averaged over five years was 649  $\text{gC m}^{-2}$ , which was approximately 24% higher than that reported by Shim et al. (2016). Overall, our estimated NEP in BAR and RIC were in the range of the result in previous studies.

### Summary and conclusions

It is crucial to understand and quantify the carbon flux to support policies to mitigate and adapt to climate change. The estimation of the CO<sub>2</sub> flux over crop fields is complex as it is affected by multiple meteorological variables and agricultural activities. This study analyzed the long-term (5 years) CO<sub>2</sub> flux over barley–rice double-cropping fields in the southern-most Korean Peninsula.

The annual variation in the daily average NEE showed a bimodal pattern with two strong negative peaks in mid-April and early August, representing significant CO<sub>2</sub> uptake by barley and rice, respectively. The annual variation in the daily average GPP and Re also showed a bimodal pattern, with peaks in the barley ripening stage and rice elongation stage. The peaks of GPP were mainly driven by seasonal variations in solar radiation combined with the growth of each crop. Both Tair and Tsoil influenced Re at night.

In contrast to BAR, irrigation is essential and can control the soil Re in RIC. The relative importance of



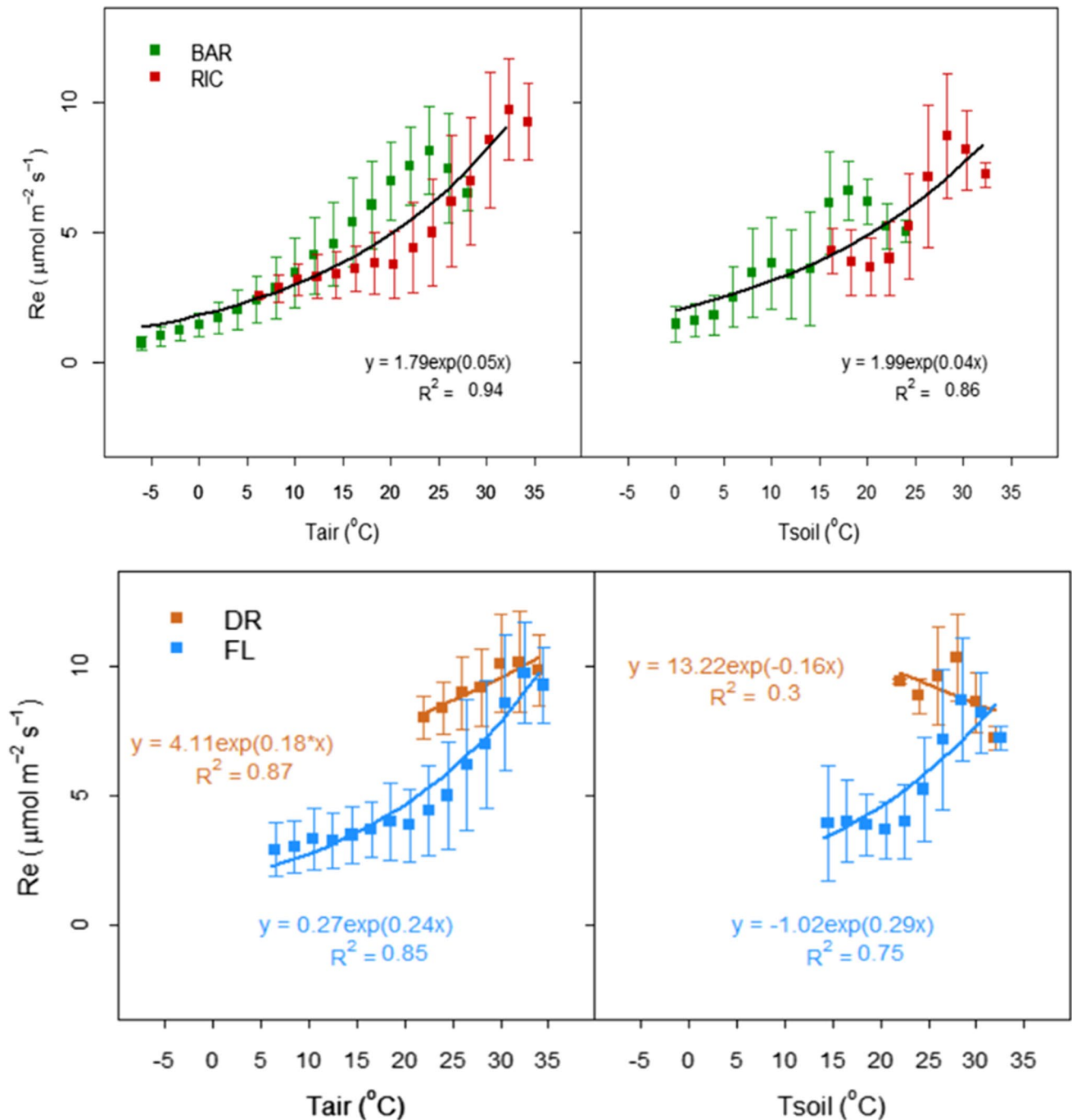


**Fig. 5** Relationship between daily average  $Re$  and  $T_{\text{air}}$  and  $T_{\text{soil}}$  at nighttime, during BAR and RIC (upper panel) and DR and FL (bottom panel), using data binned into  $2^{\circ}\text{C}$  intervals. Error bars indicate

the 1-sigma standard deviation of flux data in each bin. The black line indicates a modeled response function for  $T_{\text{air}}$  and  $T_{\text{soil}}$  with a  $Q_{10}$  of 1.93 and 1.73, respectively, during all crop growing seasons

temperature was about a factor of 2–3 higher in RIC than in BAR because of the role of irrigated water, reducing the significance of SHF. The average  $Re$  in DR was approximately  $3 \mu\text{mol m}^{-2} \text{s}^{-1}$ , which is higher than that in FL. This can be explained by the inhibition of soil respiration during FL.

The annual NEP showed a continuous decrease each year. The NEP was  $315 \text{ gC m}^{-2}$  and  $349 \text{ gC m}^{-2}$  for BAR and RIC, respectively, and  $649 \text{ gC m}^{-2}$  for the annual total. These values were comparable with those measured in other barley–rice double-cropping fields in a similar range of latitude ( $34^{\circ}\text{N}$ – $35^{\circ}\text{N}$ ) using the EC system.

**Fig. 6** Relationship between Re and SHF in BAR and RIC, including DR and FL, using data binned into 2 °C intervals: (a) for the whole range of Tair and (b) within the range of 20 °C < Tair < 30 °C. Error bars indicate the 1-sigma standard deviation of flux data in each bin

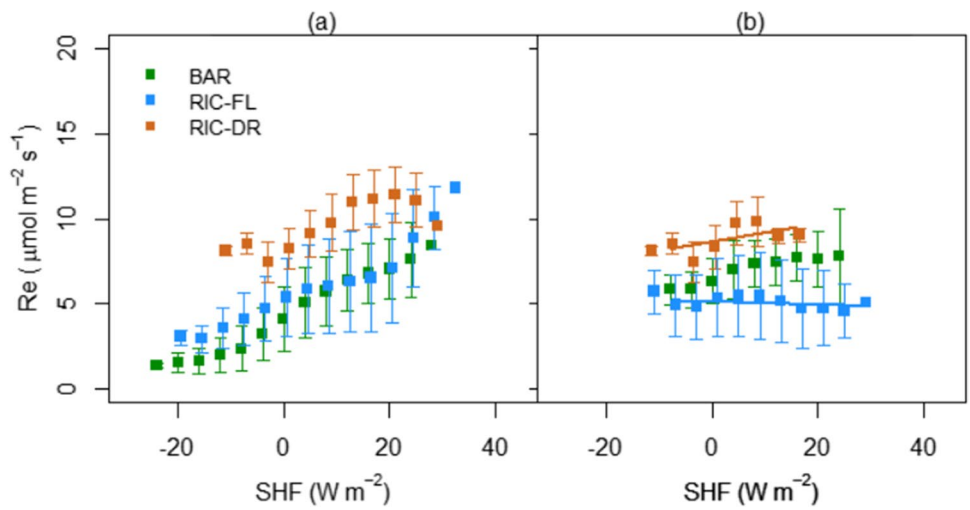


**Fig. 7** Annual accumulated CO<sub>2</sub> flux from 2016 to 2020 (excluding 2017)

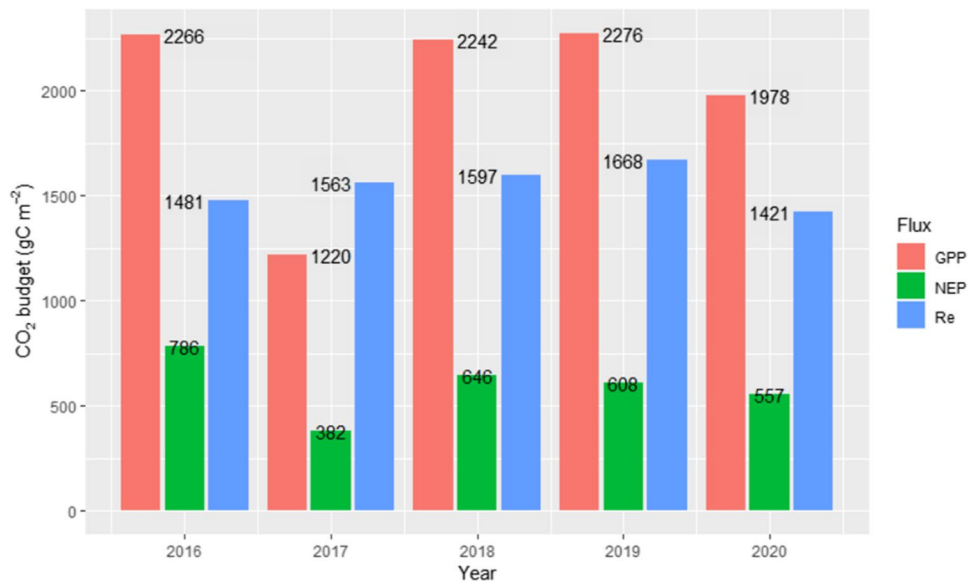


**Table 2** Accumulated NEP measured over the barley–rice double-cropping field located from 34°N to 35°N

References	Site location	Period	Annually accumulated fluxes (gC m <sup>-2</sup> )								
			BAR			RIC			Annual		
			NEP	GPP	Re	NEP	GPP	Re	NEP	GPP	Re
Takimoto et al. (2010)	34°32'N 135°54'E	November 28, 2004–November 27, 2008	255	538	283	350	727	377	545	1265	720
Kwon et al. (2010) <sup>1</sup>	34°33'N 126°34'E	2006–2008	63	481	544	121	840	719	58	1321	1263
Min et al. (2014)	35°44'N 126°51'E	October 27, 2011–June 8, 2012	348	663	315	-	-	-	-	-	-
Shim et al. (2014)	35°44'N 126°51'E	June 9, 2012–October 20, 2012	-	-	-	229	743	514	-	-	-
Shim et al. (2016)	35°44'N 126°51'E	October 22, 2013–October 18, 2014	185	638	453	442	1018	576	603	1665	1062
This study <sup>2</sup>	34°45'N 127°12'E	January 1, 2016–December 31, 2020	315	1007	692	349	1115	766	649	2191	1542

<sup>1</sup>Fluxes were averaged for 3-year measurements. The sum of fluxes in winter and spring is designated for BAR, and summer and fall for RIC

<sup>2</sup>Except 2017, owing to long-term missing fluxes

Understanding the CO<sub>2</sub> cycle over a double-crop field is complicated. The CO<sub>2</sub> flux is influenced by ecological mechanisms, anthropogenic activities, and crop type. We expect the results of our long-term study to support the estimation of the global carbon budget and to support the development of climate change mitigation and adaptation policy in the agricultural sector, especially in barley–rice double-cropping fields.

**Supplementary Information** The online version contains supplementary material available at <https://doi.org/10.1007/s00484-022-02341-y>.

**Acknowledgements** The authors thank the National Institute of Meteorological Sciences researchers for providing us with access to observation data of the Boseong Standard Weather Observatory and pictures in Supplementary Fig. 1. The following tools were used for figures: Google Earth and QGIS for Fig. 1; the R-package of “openair” and “ggplot2” for Supplementary Fig. 3 and Fig. 7, respectively; the flux footprint prediction tool of Kljun et al. (2015) for Supplementary Fig. 4.

**Funding** This study was supported by the Basic Science Research Program through the National Research (NRF), funded by the Ministry of Education (No. 2020R111A1A01055060 and 2020R1A6A1A03044834).

**Data availability** The raw measurement datasets are fully available from the Korean Meteorological Administration upon calling +82-64-780-6608.

## Declarations

**Competing interests** The authors declare no competing interests.

## References

- Alberto MCR, Wassmann R, Hirano T, Miyata A, Kumar A, Padre A, Amante M (2009) CO<sub>2</sub>/heat fluxes in rice fields: comparative assessment of flooded and non-flooded fields in the Philippines. *Agr Forest Meteorol* 149(10):1737–1750. <https://doi.org/10.1016/j.agrformet.2009.06.003>
- Arevalo CBM, Bhatti JS, Chang SX, Sidders D (2011) Land use change effects on ecosystem carbon balance: from agricultural to hybrid poplar plantation. *Agr Ecosyst Environ* 141(3–4):342–349. <https://doi.org/10.1016/j.agee.2011.03.013>
- Baldocchi DD (2003) Assessing the eddy covariance technique for evaluating carbon dioxide exchange rates of ecosystems: past, present and future. *Global Change Biol* 9(4):479–492. <https://doi.org/10.1046/j.1365-2486.2003.00629.x>
- Baldocchi DD (2020) How eddy covariance flux measurements have contributed to our understanding of Global Change Biology. *Global Change Biol* 26(1):242–260. <https://doi.org/10.1111/gcb.14807>
- Baldocchi D, Falge E, Gu LH, Olson R, Hollinger D, Running S, Anthoni P, Bernhofer C, Davis K, Evans R, Fuentes J, Goldstein A, Katul G, Law B, Lee XH, Malhi Y, Meyers T, Munger W, Oechel WUKTP, Pilegaard K, Schmid HP, Valentini R, Verma S, Vesala T, Wilson K, Wofsy S (2001) FLUXNET: a new tool to study the temporal and spatial variability of ecosystem-scale carbon dioxide, water vapor, and energy flux densities. *B Am Meteorol Soc* 82(11):2415–2434
- Bhatia A, Aggarwal PK, Jain N, Pathak H (2012) Greenhouse gas emission from rice- and wheat-growing areas in India: spatial analysis and upscaling. *Greenh Gases* 2(2):115–125. <https://doi.org/10.1002/ghg.1272>
- Chaichana N, Bellingrath-Kimura SD, Komiya S, Fujii Y, Noborio K, Dietrich O, Pakoktom T (2018) Comparison of closed chamber and eddy covariance methods to improve the understanding of methane fluxes from rice paddy fields in Japan. *Atmosphere-Basel* 9 (9) ARTN 35610.3390/atmos9090356
- Diak GR, Mecikalski JR, Anderson MC, Norman JM, Kustas WP, Torn RD, DeWolf RL (2004) Estimating land surface energy budgets from space – review and current efforts at the University of Wisconsin-Madison and USDA-ARS. *B Am Meteorol Soc* 85(1):65. <https://doi.org/10.1175/Bams-85-1-65>
- El-Madany TS, Carrara A, Martin MP, Moreno G, Kolle O, Pacheco-Labrador J, Weber U, Wutzler T, Reichstein M, Migliavacca M (2020) Drought and heatwave impacts on semi-arid ecosystems’ carbon fluxes along a precipitation gradient. *Philos T R Soc B* 375 (1810) ARTN 2019051910.1098/rstb.2019.0519
- Falge E, Baldocchi D, Tenhunen J, Aubinet M, Bakwin P, Berbigier P, Bernhofer C, Burba G, Clement R, Davis K, Aelbers J, HGoldstein A, Grelle A, Granier A, Guðmundsson J, Hollinger D, Kowalski A, Katul G, Law B, Malhi Y, Meyers T, Monson R, Munger JW, Oechel W, Paw U KT, Pilegaard K, Rannik U, Rebmann C, Suyker A, Valentini R, Wilson k, Wofsy S (2002) Seasonality of ecosystem respiration and gross primary production as derived from FLUXNET measurements. *Agric For Meteorol* 113(1–4):53–74. [https://doi.org/10.1016/S0168-1923\(02\)00102-8](https://doi.org/10.1016/S0168-1923(02)00102-8)
- Gash JHC, Culf AD (1996) Applying a linear detrend to eddy correlation data in real time. *Bound-Lay Meteorol* 79(3):301–306
- Gromping U (2006) Relative importance for linear regression in R: the package relaimpo. *J Stat Softw* 17 (1) <https://doi.org/10.18637/jss.v017.i01>
- Hong J, Kim J, Moon BK, Kim H, Kim B (2001) Exchange of momentum, energy and carbon dioxide in rice paddy. *Atmosphere Korean J Meteorol Soc* 11(3):573–576 In Korean with English abstract
- Horst TW, Weil JC (1992) Footprint estimation for scalar flux measurements in the atmospheric surface layer. *Bound-Layer Meteorol* 59(3):279–296. <https://doi.org/10.1007/BF00119817>
- IPCC (2021) Climate Change 2021: The Physical Science Basis. Contribution of Working Group I to the Sixth Assessment Report of the Intergovernmental Panel on Climate Change. Cambridge University Press, Cambridge, United Kingdom and New York, NY, USA. <https://doi.org/10.1017/9781009157896>
- Kanianska R (2016) Agriculture and its impact on land-use, environment, and ecosystem services. <https://www.intechopen.com/chapters/51201>. <https://doi.org/10.5772/63719>
- Kljun N, Calanca P, Rotach MW, Schmid HP (2015) A simple two-dimensional parameterisation for Flux Footprint Prediction (FFP). *Geosci Model Dev* 8(11):3695–3713. <https://doi.org/10.5194/gmd-8-3695-2015>
- Kwon H, Kim J, Hong J, Lim JH (2010) Influence of the Asian monsoon on net ecosystem carbon exchange in two major ecosystems in Korea. *Biogeosciences* 7(5):1493–1504. <https://doi.org/10.5194/bg-7-1493-2010>
- Liu Y, Wan KY, Tao Y, Li ZG, Zhang GS, Li SL, Chen F (2013) Carbon dioxide flux from rice paddy soils in Central China: effects of intermittent flooding and draining cycles. *Plos One* 8(2):e56562. <https://doi.org/10.1371/journal.pone.0056562>
- Lohila A, Aurela M, Tuovinen JP, Laurila T (2004) Annual CO<sub>2</sub> exchange of a peat field growing spring barley or perennial forage grass. *J Geophys Res-Atmos* 109(D18):D18116. <https://doi.org/10.1029/2004jd004715>

- Mauder M, Foken T (2006) Impact of post-field data processing on eddy covariance flux estimates and energy balance closure. *Meteorol Z* 15(6):597–609
- Mejjide A, de la Rua C, Guillaume T, Roll A, Hassler E, Stiegler C, Tjoa A, June T, Corre MD, Veldkamp E, Knohl A (2020) Measured greenhouse gas budgets challenge emission savings from palm-oil biodiesel. *Nat Commun* 11(1):1089. <https://doi.org/10.1038/s41467-020-14852-6>
- Min SH, Shim KM, Kim YS, Hwang H, Jung MP, Choi IT (2014) Seasonal variation of CO<sub>2</sub> exchange during the barley growing season at a rice-barley double cropping paddy field in Gimje. *Korea Korean J Agr Forest Meteorol* 16(2):137–145. <https://doi.org/10.5532/KJAFM.2014.16.2.137>In Korean with English Abstract
- Miyata A, Leuning R, Denmead OT, Kim J, Harazono Y (2000) Carbon dioxide and methane fluxes from an intermittently flooded paddy field. *Agr Forest Meteorol* 102(4):287–303. [https://doi.org/10.1016/S0168-1923\(00\)00092-7](https://doi.org/10.1016/S0168-1923(00)00092-7)
- Miyata A, Iwata T, Nagai H, Yamada T, Yoshikoshi H, Mano M, Ono K, Han GH, Harazono Y, Ohtaki E, Baten MA, Inohara S, Takimoto T, Saito M (2005) Seasonal variation of carbon dioxide and methane fluxes at single cropping paddy fields in central and western Japan. *Phyton-Ann Rei Bot A* 45(4):89–97
- Moncrieff JB, Massheder JM, deBruin H, Elbers J, Friborg T, Heusinkveld B, Kabat P, Scott S, Soegaard H, Verhoef A (1997) A system to measure surface fluxes of momentum sensible heat water vapour and carbon dioxide. *J Hydrol* 188(1–4):589–611
- Moncrieff JB, Clement R, Finnigan J, Meyers T (2004) Averaging, detrending and filtering of eddy covariance time series. In: Lee X, Massman WJ, Law BE (eds) *Handbook of micrometeorology: a guide for surface flux measurements*. Kluwer Academic, Dordrecht, pp 7–31
- Moon BK, Hong J, Lee BR, Yun JI, Park EW, Kim J (2003) CO<sub>2</sub> and energy exchange in a rice paddy for the growing season of 2002 in Hari. *Korea Korean J Agr Forest Meteorol* 5(2):51–60 In Korean with English abstract
- Moyano FE, Kutsch WL, Schulze ED (2007) Response of mycorrhizal, rhizosphere and soil basal respiration to temperature and photosynthesis in a barley field. *Soil Biol Biochem* 39(4):843–853. <https://doi.org/10.1016/j.soilbio.2006.10.001>
- Newton AC, Flavell AJ, Timothy G, Leat P, Mullholland B, Ramsay L, Revoredo-Giha C, Russell J, Steffenson B, Swanston JS, William T, Waugh R, White P, Bingham I (2011) Crops that feed the world 4. Barley: a resilient crop? Strengths and weaknesses in the context of food security. *Food Secur* 3(2):141–178. <https://doi.org/10.1007/s12571-011-0126-3>
- Nishimura S, Yonemura S, Minamikawa K, Yagi K (2015) Seasonal and diurnal variations in net carbon dioxide flux throughout the year from soil in paddy field. *J Geophys Res-Biogeosci* 120(1):63–76. <https://doi.org/10.1002/2014jg002746>
- Papale D, Reichstein M, Aubinet M, Canfora E, Bernhofer C, Kutsch W, Longdoz B, Rambal S, Valentini R, Vesala T, Yakir D (2006) Towards a standardized processing of Net Ecosystem Exchange measured with eddy covariance technique: algorithms and uncertainty estimation. *Biogeosciences* 3(4):571–583. <https://doi.org/10.5194/bg-3-571-2006>
- Park C, Schade GW (2016) Anthropogenic and biogenic features of long-term measured CO<sub>2</sub> flux in North Downtown Houston. *Texas J Environ Qual* 45(1):253–265
- Park C, Lee YT, Lee SH (2021) Characteristics of atmospheric CO<sub>2</sub> fluxes and the estimation of their potential sources around Boseong Standard Weather Observatory (BSWO). *Atmos Environ* 252:118340. <https://doi.org/10.1016/j.atmosenv.2021.118340>
- Pielke RA, Pitman A, Niyogi D, Mahmood R, McAlpine C, Hossain F, Goldewijk KK, Nair U, Betts R, Fall S, Reichstein M, Kabat P, de Noblet N (2011) Land use/land cover changes and climate: modeling analysis and observational evidence. *Wires Clim Change* 2(6):828–850. <https://doi.org/10.1002/wcc.144>
- Powell TL, Bracho R, Li JH, Dore S, Hinkle CR, Drake BG (2006) Environmental controls over net ecosystem carbon exchange of scrub oak in central Florida. *Agr Forest Meteorol* 141(1):19–34. <https://doi.org/10.1016/j.agrformet.2006.09.002>
- Poyda A, Reinsch T, Skinner RH, Kluss C, Loges R, Taube F (2017) Comparing chamber and eddy covariance based net ecosystem CO<sub>2</sub> exchange of fen soils. *J Plant Nutr Soil Sc* 180(2):252–266. <https://doi.org/10.1002/jpln.201600447>
- Prescher AK, Grunwald T, Bernhofer C (2010) Land use regulates carbon budgets in eastern Germany: from NEE to NBP. *Agr Forest Meteorol* 150(7–8):1016–1025. <https://doi.org/10.1016/j.agrformet.2010.03.008>
- Reichstein M, Falge E, Baldocchi D, Papale D, Aubinet M, Berbigier P, Bernhofer C, Buchmann N, Gilmanov T, Granier A, Grunwald T, Havrankova K, Ilvesniemi H, Janous D, Knohl A, Laurila T, Lohila A, Loustau D, Matteucci G, Meyers T, Miglietta F, Ourcival JM, Pumpanen J, Rambal S, Rotenberg E, Sanz M, Tenhunen J, Seufert G, Vaccari F, Vesala T, Yakir D, Valentini R (2005) On the separation of net ecosystem exchange into assimilation and ecosystem respiration: review and improved algorithm. *Global Change Biol* 11(9):1424–1439. <https://doi.org/10.1111/j.1365-2486.2005.001002.x>
- Ren XE, Wang QX, Tong CL, Wu JS, Wang KL, Zhu YL, Lin ZJ, Masataka W, Tang GY (2007) Estimation of soil respiration in a paddy ecosystem in the subtropical region of China. *Chinese Sci Bull* 52(19):2722–2730. <https://doi.org/10.1007/s11434-007-0346-2>
- Ryan MG (1991) Effects of climate change on plant respiration. *Ecol Appl* 1(2):157–167. <https://doi.org/10.2307/1941808>
- Saito M, Miyata A, Nagai H, Yamada T (2005) Seasonal variation of carbon dioxide exchange in rice paddy field in Japan. *Agr Forest Meteorol* 135(1–4):93–109. <https://doi.org/10.1016/j.agrformet.2005.10.007>
- Saito M, Kato T, Tang Y (2009) Temperature controls ecosystem CO<sub>2</sub> exchange of an alpine meadow on the northeastern Tibetan Plateau. *Global Change Biol* 15(1):221–228. <https://doi.org/10.1111/j.1365-2486.2008.01713.x>
- Schmitt M, Bahn M, Wohlfahrt G, Tappeiner U, Cernusca A (2010) Land use affects the net ecosystem CO<sub>2</sub> exchange and its components in mountain grasslands. *Biogeosciences* 7(8):2297–2309. <https://doi.org/10.5194/bg-7-2297-2010>
- Schneider J, Kutzbach L, Wilmking M (2012) Carbon dioxide exchange fluxes of a boreal peatland over a complete growing season, Komi Republic. *NW Russia Biogeochemistry* 111(1–3):485–513. <https://doi.org/10.1007/s10533-011-9684-x>
- Shim KM, Min SH, Kim YS, Jeong MP, Hwang H, Kim SC, So KH (2014) Environmental controls on net ecosystem CO<sub>2</sub> exchange during a rice growing season at a rice-barley double cropping paddy field in Gimje Korea. *J Clim Change Res* 5(1):71–81. <https://doi.org/10.15531/KSCCR.2014.5.1.71>
- Shim KM, Min SH, Kim YS, Jung MP, Choi IT, Kang KK (2016) Comparison of carbon budget between rice-barley double cropping and rice mono cropping field in Gimje. *South Korea Korean J Agr Forest Meteorol* 18(4):337–347. <https://doi.org/10.5532/KJAFM.2016.18.4.337>In Korean with English abstract
- Smith P, Soussana JF, Angers D, Schipper L, Chenu C, Rasse DP, Batjes NH, van Egmond F, McNeill S, Kuhnert M, Arias-Navarro C, Olesen JE, Chirinda N, Fornara D, Wollenberg E, Alvarofuentes J, Sanz-Cobena A, Klumpp K (2020) How to measure, report and verify soil carbon change to realize the potential of soil carbon sequestration for atmospheric greenhouse gas removal. *Global Change Biol* 26(1):219–241. <https://doi.org/10.1111/gcb.14815>

- Stoy PC, Mauder M, Foken T, Marcolla B, Boegh E, Ibrom A, Arain MA, Arneth A, Aurela M, Bernhofer C, Cescatti A, Dellwik E, Duce P, Gianelle D, van Gorsel E, Kiely G, Knohl A, Margolis H, McCaughey H, Merbold L, Montagnani L, Papale D, Reichstein M, Saunders M, Serrano-Ortiz P, Sottocornola M, Spano D, Vaccari F, Varlagin A (2013) A data-driven analysis of energy balance closure across FLUXNET research sites: the role of landscape scale heterogeneity. *Agr Forest Meteorol* 171:137–152. <https://doi.org/10.1016/j.agrformet.2012.11.004>
- Takimoto T, Iwata T, Yamamoto S, Miura T (2010) Characteristics of CO<sub>2</sub> and CH<sub>4</sub> flux at barley-rice double cropping field in southern part of Okayama. *J Agr Meteorol* 66(3):181–191. <https://doi.org/10.2480/agrmet.66.3.5>In Japanese with English abstract
- Testi L, Orgaz F, Villalobos F (2008) Carbon exchange and water use efficiency of a growing, irrigated olive orchard. *Environ Exp Bot* 63(1–3):168–177. <https://doi.org/10.1016/j.envexpbot.2007.11.006>
- Tseng KH, Tsai JL, Alagesan A, Tsuang BJ, Yao MH, Kuo PH (2010) Determination of methane and carbon dioxide fluxes during the rice maturity period in Taiwan by combining profile and eddy covariance measurements. *Agr Forest Meteorol* 150(6):852–859. <https://doi.org/10.1016/j.agrformet.2010.04.007>
- Velasco E, Roth M, Tan SH, Quak M, Nabarro SDA, Norford L (2013) The role of vegetation in the CO<sub>2</sub> flux from a tropical urban neighbourhood. *Atmos Chem Phys* 13(20):10185–10202
- Vickers D, Mahrt L (1997) Quality control and flux sampling problems for tower and aircraft data. *J Atmos Oceanic Tech* 14(3):512–526
- Webb EK, Pearman GI, Leuning R (1980) Correction of flux measurements for density effects due to heat and water-vapor transfer. *Q J R Meteorol Soc* 106(447):85–100
- Wilczak JM, Oncley SP, Stage SA (2001) Sonic anemometer tilt correction algorithms. *Bound-Lay Meteorol* 99(1):127–150. <https://doi.org/10.1023/A:1018966204465>
- Wilson KB, Baldocchi DD (2000) Seasonal and interannual variability of energy fluxes over a broadleaved temperate deciduous forest in North America. *Agr Forest Meteorol* 100(1):1–18. [https://doi.org/10.1016/S0168-1923\(99\)00088-X](https://doi.org/10.1016/S0168-1923(99)00088-X)
- Wohlfahrt G, Galvagno M (2017) Revisiting the choice of the driving temperature for eddy covariance CO<sub>2</sub> flux partitioning. *Agric For Meteorol* 237–238:135–142. <https://doi.org/10.1016/j.agrformet.2017.02.012>
- Wutzler T, Lucas-Moffat A, Migliavacca M, Knauer J, Sickel K, Sigut L, Menzer O, Reichstein M (2018) Basic and extensible post-processing of eddy covariance flux data with REdDyProc. *Biogeosciences* 15(16):5015–5030. <https://doi.org/10.5194/bg-15-5015-2018>

Springer Nature or its licensor holds exclusive rights to this article under a publishing agreement with the author(s) or other rightsholder(s); author self-archiving of the accepted manuscript version of this article is solely governed by the terms of such publishing agreement and applicable law.